Onset and stabilization of delay-induced instabilities in piezoelectric digital vibration absorbers

Journal Title
XX(X):1–15

DOI: 10.1177/ToBeAssigned
www.sagepub.com/
SAGE

Ghislain Raze[1], Jennifer Dietrich[1] and Gaetan Kerschen[1]

Abstract

The stability of a piezoelectric structure controlled by a digital vibration absorber emulating a shunt circuit is investigated in this work. The formalism of feedback control theory is used to demonstrate that systems with a low electromechanical coupling are prone to delay-induced instabilities entailed by the sampling procedure of the digital unit. An explicit relation is derived between the effective electromechanical coupling factor and the maximum sampling period guaranteeing a stable controlled system. Since this sampling period may be impractically small, a simple modification procedure of the emulated admittance of the shunt circuit is proposed in order to counteract the effect of delays by anticipation. The theoretical developments are experimentally validated on a clamped-free piezoelectric beam.

Keywords

vibration mitigation, piezoelectric shunt damping, digital vibration absorber, delay-induced instabilities, stabilization

Introduction

Engineering structures from various disciplines tend to be lighter or more slender, which usually goes along with smaller structural damping and increased susceptibility to vibrations, threatening structural integrity. Piezoelectric shunt damping is often considered as one potential solution to this issue. It was originally proposed by Forward (1979), and formalized by Hagood and von Flotow (1991). The working principle of piezoelectric shunt damping is based on the capability of piezoelectric transducers to convert a part of their mechanical energy into electrical energy. The latter can be dissipated by connecting a shunt circuit to the electrodes of the transducer. Shunts of resistive or resonant types (composed of a resistor and an inductor, arranged either in series or in parallel) are commonly used. When properly tuned, the latter exhibits better performance in terms of vibration reduction than the former. Negative capacitances can also be used to improve performance, but the introduction of such a component in the circuit requires a careful stability analysis (Berardengo et al. 2018). The realization of resonant shunts may be challenging for several reasons. First, the required inductance may be impractically large. Second, the performance of the piezoelectric shunt is highly sensitive to the values of the electrical components. Any misevaluation or time variation of the system characteristics will result in sub-optimal performance, rectified by time-consuming manual modifications of the electrical parameters.

Fleming et al. (2000); Fleming (2004) introduced the concept of synthetic impedance as an alternative solution. The combination of a digital signal processor with a current source makes the realization of an arbitrary impedance possible. The synthetic impedance is an attractive option to realize shunt damping circuits owing to its versatility. This nonetheless comes at the expense of the need for powering the digital unit and its associated electronics. Since it was proposed, the application of piezoelectric shunt damping with a digital vibration absorber (DVA) was used in several works. Fleming and Moheimani (2002) and Plíva et al. (2007) developed architectures using pulse width modulation in order to simplify the driving electronics. Niederberger et al. (2004) implemented an adaptive impedance with a DVA in order to improve the robustness of the control system. Giorgio et al. (2009) and Rosi (2010) used digital controllers

[1]Space Structures and Systems Laboratory, Aerospace and Mechanical Engineering Department, University of Liège

Corresponding author:
Ghislain Raze, Space Structures and Systems Laboratory, Aerospace and Mechanical Engineering Department, University of Liège Liège, Belgium

Email: g.raze@uliege.be

to validate their theoretical developments on piezoelectric damping with electrical networks. Matten et al. (2014), Nečásek et al. (2016, 2017) and Silva (2018) investigated various electronic architectures to implement a DVA, and discussed how to set up its analog and digital parts. Dal Bo et al. (2019) configured a digital unit to realize vibration absorbers with swept and switched characteristics. Recently, this concept was applied to metamaterials by Sugino et al. (2018, 2020) and Yi et al. (2020), and to nonlinear shunt damping (Raze et al. 2020).

In the active control terminology, the DVA is equivalent to a control system with a self-sensing actuator, and it implements a passive control law. From a theoretical standpoint, a passive control law features unconditional stability of the controlled system (Moheimani et al. 2003). If the problem is cast into a feedback control one, the system exhibits an infinite gain margin but a finite phase margin. Because a digital unit needs to sample the signals it is working with, unavoidable delays occur in the control loop. These delays introduce a phase lag which may destabilize the controlled system if they are too large. Nečásek et al. (2016) and Sugino et al. (2018) pinpointed the fact that in some cases a DVA needs to have a sampling frequency much higher than the typical frequencies of interest. The authors also noted that delay-induced instabilities may arise when using a DVA for surprisingly small sampling periods, in spite of the passivity of the control law (Raze et al. 2019). It was shown in previous works that increasing the values of resistive elements helps stabilizing the system (Sugino et al. 2020). However, to the authors' knowledge, no explanation exists on the reason for the onset of such instabilities, and no systematic method was proposed to counteract them.

In this work, novel and ready-to-use formulas are provided to determine whether delay-induced instabilities can be an issue, and how to solve this issue if need be. Specifically, the purpose of this paper is to evidence 1. why a DVA may need a high sampling frequency for stability, 2. how delay-induced instabilities may arise and 3. how to counteract them. After reviewing the basics of piezoelectric shunt damping with a DVA, the possibility for instabilities of the control system is investigated. The problem is cast as a feedback control one, and a relation between the effective electromechanical coupling factor and the phase margin is derived. Values of the maximum sampling period under which the system remains stable are then deduced. A procedure to stabilize the controlled system is proposed. Upon applying this procedure, larger sampling periods may be used for the digital unit without jeopardizing stability, which is generally advantageous. The findings are experimentally validated with a piezoelectric clamped-free beam. The conclusions of this work are finally reported. In comparison to the conference paper (Raze et al. 2019), this works performs an in-depth investigation of the controlled system's dynamics, links the delay-induced instabilities to the electromechanical coupling and improves the stabilization procedure proposed therein.

Piezoelectric shunt damping with a digital vibration absorber

A single-degree-of-freedom structure to which a piezoelectric transducer is bonded is considered. The structure is excited by an external force f and responds with a displacement x. V and $\dot{q}$ (where an upper dot denotes time derivation) are the voltage across the electrodes of the transducer and the current flowing through them, respectively. The governing equations of the piezoelectric structure read

$$\begin{cases} m\ddot{x} + k_{oc}x - \theta_p q = f \\ V = \theta_p x - \dfrac{1}{C_p^\varepsilon} q \end{cases}, \tag{1}$$

where m and k_{oc} are the mass and stiffness of the structure when the transducer is open-circuited, respectively, θ_p is a piezoelectric coupling coefficient and C_p^ε is the piezoelectric capacitance at constant strain. The resonance frequency of the structure when the transducer is open-circuited ($q = 0$) is given by

$$\omega_{oc} = \sqrt{\frac{k_{oc}}{m}}, \tag{2}$$

and when the transducer is short-circuited ($V = 0$), the stiffness of the structure changes to k_{sc}, and the short-circuit resonance frequency can be found as

$$\omega_{sc} = \sqrt{\frac{k_{sc}}{m}} = \sqrt{\frac{k_{oc} - \theta_p^2 C_p^\varepsilon}{m}}. \tag{3}$$

The electromechanical coupling between the transducer and the structure can be assessed from these two frequencies with the effective electromechanical coupling factor (EEMCF) K_c, defined by

$$K_c^2 = \frac{\omega_{oc}^2 - \omega_{sc}^2}{\omega_{sc}^2}. \tag{4}$$

The dynamics of multiple-degree-of-freedom structures are also amenable to a form similar to Eq. (1) if the influence of non-resonant modes is approximately accounted for with flexibility and inertia corrections (Høgsberg and Krenk 2017), provided the frequencies of these modes are not too close to that of the targeted mode.

Upon connecting a series RL shunt to the transducer, the equations of the system become

$$\begin{cases} m\ddot{x} + k_{oc}x - \theta_p q = f \\ L\ddot{q} + R\dot{q} + \dfrac{1}{C_p^\varepsilon} q - \theta_p x = 0 \end{cases}, \tag{5}$$

where L and R are the inductance and resistance of the shunt, respectively. They can be optimized to minimize the maximum vibratory amplitude of the structure (Soltani et al. 2014; Ikegame et al. 2019). Introducing an intermediate parameter

$$r = \frac{\sqrt{64 - 16K_c^2 - 26K_c^4} - K_c^2}{8}, \tag{6}$$

the optimal electrical frequency and damping ratios are given by

$$\delta(K_c) = \sqrt{\frac{3K_c^2 - 4r + 8}{4K_c^2 + 4}} \tag{7}$$

and

$$\zeta(K_c) = \frac{\sqrt{27K_c^4 + K_c^2(80 - 48r) - 64(r-1)}}{\sqrt{2}\,(5K_c^2 + 8)}, \tag{8}$$

respectively. The optimal inductance and resistance are then

$$L = \frac{1}{\delta^2(K_c)\omega_{oc}^2 C_p^\varepsilon} \tag{9}$$

and

$$R = \frac{2\zeta(K_c)}{\delta(K_c)\omega_{oc}C_p^\varepsilon}, \tag{10}$$

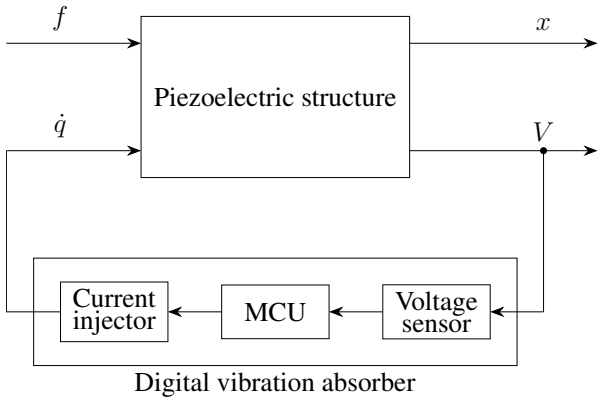

Figure 1. General working principle of the DVA.

Delay-induced instabilities

The purpose of this section is to study the stability of a system composed of a piezoelectric structure controlled by a DVA. Using the theory of feedback control (Franklin et al. 2015), it is demonstrated that the system can be sensitive to delays induced by the sampling made by the digital unit.

Delays induced by the sampling procedure

Fig. 2 depicts a schematic representation of the process undergone by an input signal $u(t)$ (typically, the piezoelectric voltage) to be transformed into an output signal $y(t)$ (typically, the piezoelectric current) by a digital unit (Franklin et al. 1998).

A sample-and-hold circuit holds the input signal $u(t)$ constant at specific times, multiples of the sampling period τ. The signal is then quantized, and the MCU operates on it to emulate the desired admittance. This signal being discrete, a discrete input-output transfer function must thus be employed. Tustin's method (Tustin 1947) is used to discretize the continuous transfer function to be emulated. If the latter is given by $Y_s(s)$, a discrete z-transform $Y_{s,d}(z)$ is obtained by substituting the s variable by a bilinear function of the complex variable z as

$$Y_{s,d}(z) = Y_s(s)|_{s=\frac{2}{\tau}\frac{z-1}{z+1}}. \tag{11}$$

This transfer function can then readily be translated into a recurrence equation (Franklin et al. 1998). The resulting output signal is also a discrete signal. It is applied to the continuous system by holding its value constant for the sample interval by a zero-order hold (ZOH), which keeps the output signal constant over a whole sampling interval.

If the MCU operates at a high enough clock frequency relative to the sampling frequency, it may be considered that the digitization of the input signal and computation of the output signal occur instantaneously at each sampling time, i.e., latency is neglected. The differences between the continuous transfer function and the digital one then principally comes from the delay brought by the ZOH, as well as the frequency warping stemming from the discretization of the transfer function.

An example relating the input and output signals when the MCU implements a simple unity gain ($Y_s = 1$) is featured in Fig. 3. In this case, a continuous average of this output signal looks identical to the input signal but delayed by $\tau/2$.

Open-loop analysis

Open-loop transfer function The stability of the nominal controlled system (i.e., without delays) is conditioned upon that of the unforced system ($f = 0$). In this case, the Laplace transform of Eq. (1) gives a relation between the

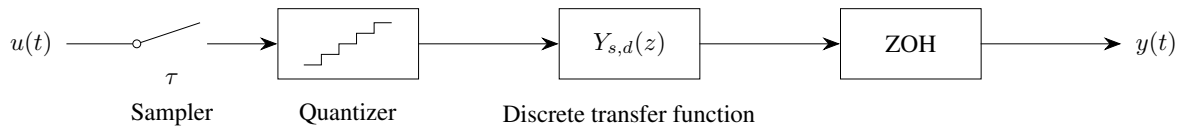

Figure 2. Block diagram representation of the input/output relation in a digital system.

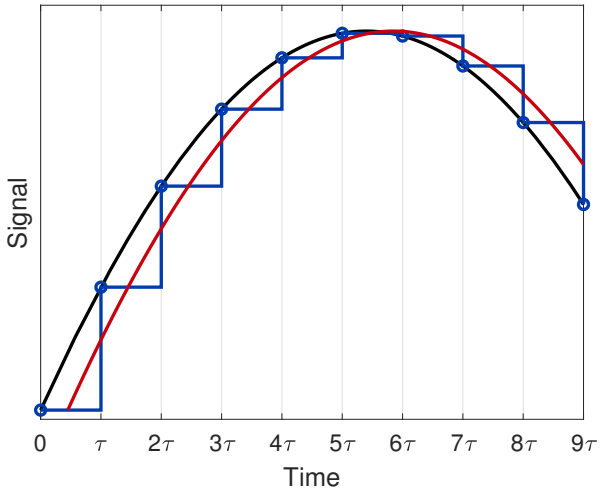

Figure 3. Signals in the MCU when it operates as a simple unity gain: input signal (—), output signal (—) and continuous average of the output signal (—).

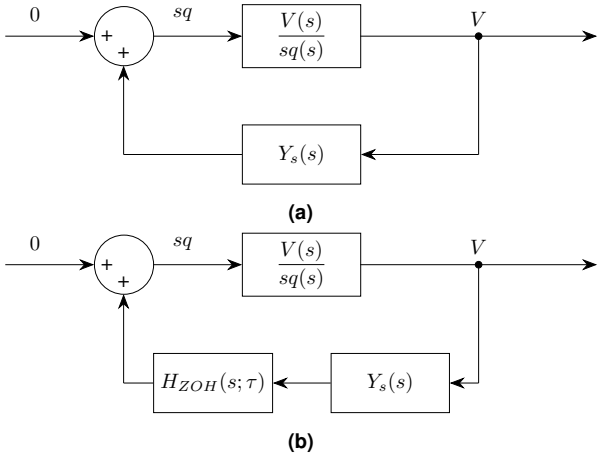

Figure 4. Block diagram representation of the nominal (a) and delayed (b) controlled systems.

piezoelectric voltage and charge (using Eqs. (2) and (3))

$$\frac{q}{V} = -C_p^\varepsilon \left(1 - \frac{C_p^\varepsilon \theta_p^2}{ms^2 + k_{oc}}\right)^{-1} = -C_p^\varepsilon \left(1 - \frac{\omega_{oc}^2 - \omega_{sc}^2}{s^2 + \omega_{oc}^2}\right)^{-1} = -C_p^\varepsilon \frac{s^2 + \omega_{oc}^2}{s^2 + \omega_{sc}^2}. \quad (12)$$

This transfer function is usually called the dynamic capacitance (Preumont 2011). Moreover, connecting an admittance $Y_s(s)$ to the electrodes of the transducer imposes the relation

$$sq = Y_s(s)V = \frac{1}{Ls + R}V \quad (13)$$

in the case of a series RL shunt. This suggests that the dynamics of the unforced controlled system may be represented with the feedback diagram depicted in Fig. 4(a).

Using Eqs. (12) and (13), one may form the open-loop transfer function H associated with this feedback loop

$$H(s) = -\frac{V(s)}{sq(s)}Y_s(s) = \frac{1}{C_p^\varepsilon}\frac{s^2 + \omega_{sc}^2}{s^2 + \omega_{oc}^2}\frac{1}{Ls^2 + Rs} \quad (14)$$

such that the poles of the closed-loop system may be found by solving the characteristic equation

$$1 + H(s) = 0. \quad (15)$$

By normalizing the Laplace variable with the short-circuit resonance frequency

$$\overline{s} = \frac{s}{\omega_{sc}} \quad (16)$$

and using Eqs. (4), (9), (10) and (14),

$$H(s) = H(\omega_{sc}\overline{s}) = \frac{\overline{s}^2 + 1}{\overline{s}^2 + 1 + K_c^2}\frac{1}{\frac{1}{(1 + K_c^2)\,\delta^2(K_c)}\overline{s}^2 + \frac{2\zeta(K_c)}{\delta(K_c)\sqrt{1 + K_c^2}}\overline{s}}, \quad (17)$$

the coefficients of the open-loop transfer function depend only on the EEMCF (since δ and ζ are sole functions of it). This parameter is thus expected to play an important role in stability.

Fig. 5(a) features Bode plots of the open-loop transfer function given in Eq. (17) for various values of K_c around the short- and open-circuit resonance frequencies. The system has an infinite gain margin because the phase never crosses -180°. There are three gain crossover frequencies, and the phase margin is calculated at the highest one (which also corresponds to the lowest phase margin). The phase margin decreases with K_c. This trend is also highlighted in Fig. 5(b).

Destabilization mechanism In order to intuitively understand why delays can cause instabilities, a simple model is now introduced. As seen previously, the delays imparted by the sampling procedure can be modeled as a pure time delay

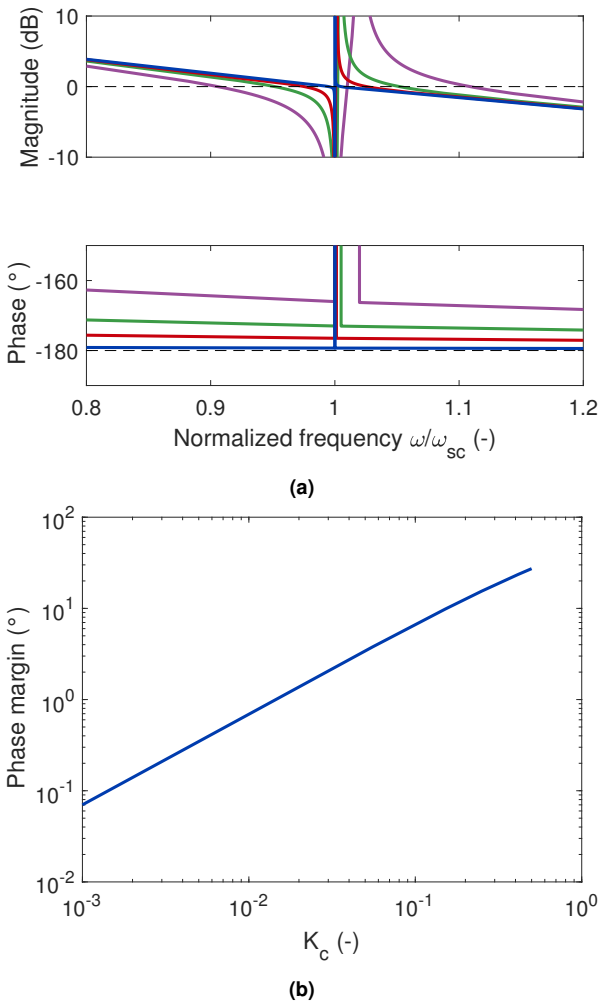

Figure 5. Bode plot of the open-loop transfer function (a): $K_c = 0.01$ (—), $K_c = 0.05$ (—), $K_c = 0.1$ (—) and $K_c = 0.2$ (—) ; phase margin as a function of K_c (b).

$\tau/2$ (Franklin et al. 1998). In the case of a series RL shunt, the piezoelectric charge and voltage are thus linked by

$$L\ddot{q}(t) + R\dot{q}(t) = V\left(t - \frac{\tau}{2}\right). \tag{18}$$

Taking the Laplace transform of this equation yields

$$q = \frac{e^{-\frac{s\tau}{2}}}{Ls^2 + Rs}V = \frac{e^{-\frac{s\tau}{2}}}{s}Y_s(s) = \frac{1}{s}Y_d(s), \tag{19}$$

where Y_s is the nominal shunt admittance and Y_d is an equivalent delayed admittance. In order to see how these two quantities differ with a simple exposition, the formulas from Thomas et al. (2012) (which are a linearization of Eqs. (9) and (10) with respect to K_c) are used to tune the inductance and the resistance.

$$L = \frac{1}{C_p^\varepsilon \omega_{oc}^2}, \qquad R = \sqrt{\frac{3}{2}}\frac{K_c}{\omega_{oc} C_p^\varepsilon}. \tag{20}$$

The admittance of the shunt evaluated at ω_{oc} is thus

$$\begin{aligned} Y_s(j\omega_{oc}) &= \frac{1}{j\omega_{oc}L + R} = \frac{C_p^\varepsilon \omega_{oc}}{j + \sqrt{\frac{3}{2}}K_c} \\ &= \frac{C_p^\varepsilon \omega_{oc}}{1 + \frac{3}{2}K_c^2}\left(\sqrt{\frac{3}{2}}K_c - j\right). \end{aligned} \tag{21}$$

An important feature of this admittance is that it has a positive real part. Indeed, the average power dissipated across an admittance Y is

$$P = \frac{1}{2}\Re\{V^* I\} = \frac{1}{2}\Re\{V^* Y V\} = \frac{1}{2}\Re\{Y\}|V|^2 \tag{22}$$

and must be positive for a passive circuit, because it dissipates true power ($\Re$ denotes the operator giving the real part of a complex number and superscript $*$ denotes complex conjugate). Another important feature is that since $K_c \ll 1$, this real part is much lower than the absolute value of the imaginary part.

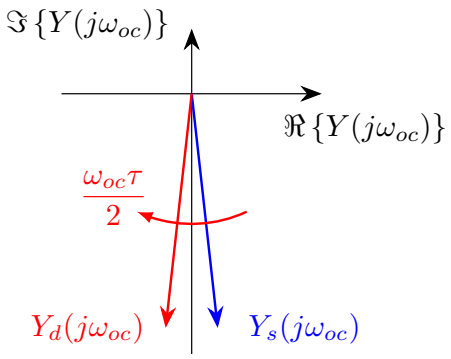

Figure 6. Representation of the admittance in the complex plane.

More quantitatively, using Eqs. (19) and (21), the delayed admittance is given by

$$\begin{aligned} &Y_d(j\omega_{oc}) \\ &= \frac{C_p^\varepsilon \omega_{oc}}{1 + \frac{3}{2}K_c^2}\left[\sqrt{\frac{3}{2}}K_c \cos\left(\frac{\omega_{oc}\tau}{2}\right) - \sin\left(\frac{\omega_{oc}\tau}{2}\right)\right. \\ &\left. -j\left(\cos\left(\frac{\omega_{oc}\tau}{2}\right) + \sqrt{\frac{3}{2}}K_c \sin\left(\frac{\omega_{oc}\tau}{2}\right)\right)\right], \end{aligned} \tag{23}$$

whose real part becomes negative when

$$\begin{aligned} \tau &= \frac{2}{\omega_{oc}}\arctan\left(\sqrt{\frac{3}{2}}K_c\right) \\ &= \frac{1}{\omega_{oc}}\left(\sqrt{6}K_c + O(K_c^3)\right) = \frac{1}{\omega_{sc}}\left(\sqrt{6}K_c + O(K_c^3)\right). \end{aligned} \tag{24}$$

Closed-loop analysis

Characteristic equation The closed-loop system when the structure is controlled by a DVA is represented in Fig. 4(b). Delays are introduced in the system by the ZOH.

Assuming the output of the ZOH is dominated by the fundamental harmonic of the frequency it is subject to, an equivalent continuous transfer function can be shown to be (Franklin et al. 1998)

$$H_{ZOH}(s;\tau) = \frac{1-e^{-\tau s}}{\tau s}. \tag{25}$$

Based on Fig. 4(b), the characteristic equation is then

$$1 - \frac{V(s)}{sq(s)} Y_s(s) H_{ZOH}(s;\tau) = 1 + H(s)\frac{1-e^{-\tau s}}{\tau s} = 0. \tag{26}$$

where H is given by Eq. (14) and is the open-loop transfer function of the system without delays, i.e., for $\tau = 0$. The roots of Eq. (26) are the poles of the closed-loop system, and all of them must have a negative real part to guarantee the stability of this system (Walton and Marshall 1987). An inherent difficulty introduced by the presence of delays is that this characteristic equation is now transcendental. For nonzero τ, the system possesses an infinity of poles which cannot be found in closed-form.

Root loci Eq. (26) can be solved numerically using homotopy: from the known solution at $\tau = 0$ (where the characteristic equation is a polynomial), the root locus can progressively be computed. At each step, starting from a known solution for a given τ, τ is incremented by $\Delta\tau$ and Eq. (26) is solved with MATLAB's routine `fsolve` using as the initial guess the solution for the previous value of τ. The procedure is then repeated until τ reaches a prescribed final value.

Fig. 7 shows root loci of the controlled system with delays for two values of K_c. The maximum value for τ is the maximum sampling period satisfying the Nyquist-Shannon sampling theorem if the system was forced at its resonant frequency ω_{sc}, π/ω_{sc}.

In all of these cases, the poles initially move to the right of the complex plane with increasing delays, and for large enough τ the highest-frequency poles cross the imaginary axis, which makes the closed-loop system unstable. As expected, the value of τ for which this instability occurs grows with K_c.

Fig. 7 does not feature all the poles of the delayed system, except for $\tau = 0$. As soon as $\tau > 0$, a countable infinite set of poles emanate from $-\infty$, but these poles are not causing instabilities, unlike those featured in Fig. 7.

Critical delays Of particular interest is the value of τ for which the poles of the closed-loop system cross the imaginary axis, signalling the onset of instability. An inconvenient feature of Eq. (26) is that this value can only be obtained by solving a transcendental equation. However, the following approximation can be made at frequencies comparatively low to the sampling frequency:

$$\begin{aligned} H_{ZOH}(s;\tau) &= \frac{1-e^{-\tau s}}{\tau s} = e^{-\frac{\tau s}{2}} \frac{e^{\frac{\tau s}{2}} - e^{-\frac{\tau s}{2}}}{\tau s} \\ &= e^{-\frac{\tau s}{2}} \frac{\sum_{k=0}^{+\infty} \left(\frac{\tau s}{2}\right)^k - \sum_{k=0}^{+\infty} \left(-\frac{\tau s}{2}\right)^k}{\tau s} \\ &= e^{-\frac{\tau s}{2}} \sum_{k=0}^{+\infty} \left(\frac{\tau s}{2}\right)^{2k} \approx e^{-\frac{\tau s}{2}}, \end{aligned} \tag{27}$$

i.e., the ZOH is nearly equivalent to a pure delay of $\tau/2$. With a pure delay model, the method of Walton and Marshall (1987) can be used to compute the characteristics roots of interest. Eq. (26) is rewritten as

$$1 + H(s)e^{-\frac{\tau s}{2}} = 0, \tag{28}$$

The time delay resulting in purely imaginary characteristic roots is noted τ_c. At this delay, a pair of complex conjugate poles or a single real pole cross the imaginary axis, possibly changing the stability of the system. Thus, $s = j\omega_c$ and $s = -j\omega_c$ satisfy the characteristic equation

$$\begin{cases} 1 + H(j\omega_c)e^{-\frac{j\omega_c\tau_c}{2}} = 0 \\ 1 + H(-j\omega_c)e^{\frac{j\omega_c\tau_c}{2}} = 0 \end{cases}. \tag{29}$$

Multiplication of these two equations yield

$$H(j\omega_c)H(-j\omega_c) = 1. \tag{30}$$

This equation is a polynomial of ω_{sc}; hence, there is a finite set of frequencies at which the poles of the closed-loop system cross the imaginary axis (Walton and Marshall 1987). The corresponding time delay τ_c can then be found using either line of Eq. (29) as

$$\tau_c = \frac{2}{\omega_c}\left[\angle - H(j\omega_c) + 2k\pi\right], \qquad k \in \mathbb{Z}, \tag{31}$$

where $\angle$ is an operator giving the phase of a complex number.

Series approximations Using Eq. (14), it can be shown that Eq. (30) is a quartic polynomial of ω_c^2. A closed-form solution can thus be obtained, but is impractically long. A more convenient form was obtained through Maclaurin series

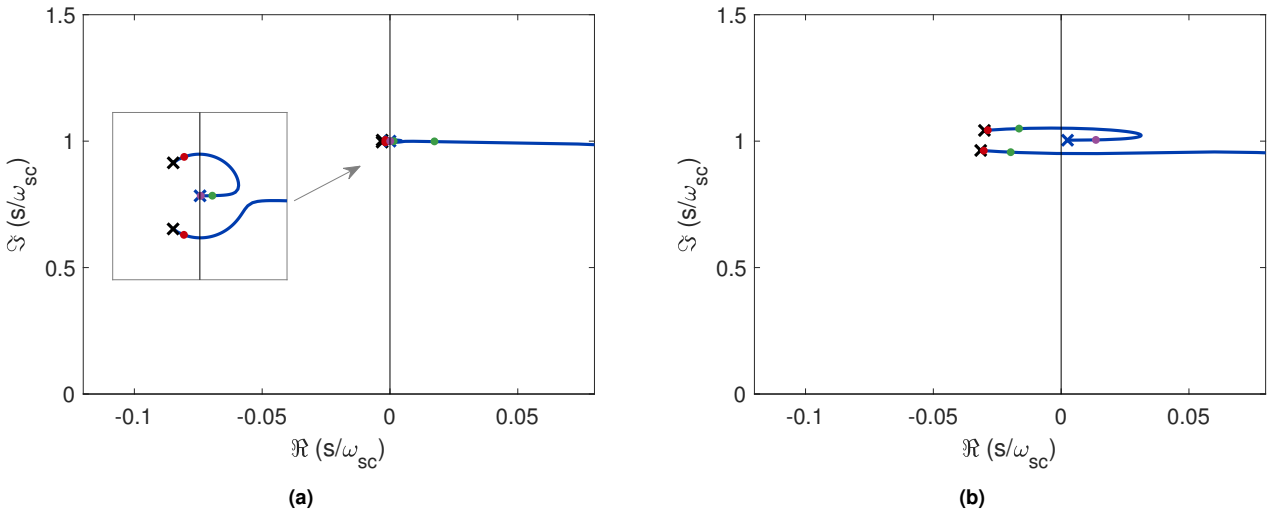

Figure 7. Root loci (parametrized by τ) of the closed-loop system with delays ($\times$: poles for $\tau = 0$, $\bullet$: $\tau = 0.01/\omega_{sc}$, $\bullet$: $\tau = 0.1/\omega_{sc}$, $\bullet$: $\tau = 1/\omega_{sc}$, $\times$: $\tau = \pi/\omega_{sc}$): $K_c = 0.01$ (a) and $K_c = 0.1$ (b).

expansion in powers of K_c of the analytical solution using Wolfram Mathematica. This provides an approximation of the critical frequencies. Among them, the one which corresponds to the minimum critical delay is given by

$$\omega_c = \omega_{sc}\left(1 + K_c + \frac{5}{8}K_c^2 + \frac{73}{128}K_c^3 + O(K_c^4)\right). \quad (32)$$

Inserting this critical frequency into Eq. (31) and expanding the result in power series of K_c gives the corresponding critical delay

$$\tau_c = \frac{1}{\omega_{sc}}\left(\sqrt{6}\left(K_c - K_c^2\right) + \frac{19}{32}\sqrt{\frac{3}{2}}K_c^3 + O(K_c^4)\right). \quad (33)$$

τ_c corresponds to the largest admissible value of sampling time for a stable closed-loop system. It may also be noted that the first-order coefficient in K_c obtained in Eq. (33) for τ_c corresponds to that of the linearized value of τ leading to a non-passive delayed admittance (Eq. (24)).

Eq. (33) indicates that the critical sampling period is governed by the EEMCF of the system, whose value is typically small ($K_c \lesssim 0.1$). Hence, the associated critical sampling frequency may be orders of magnitude larger than the characteristic frequencies of the system. Although such a trend has been exhibited for other types of vibration absorbers before (Olgac and Elmali 2000), it is an important fact that needs to be accounted for when the DVA is used to emulate a passive shunt.

The analytical approximations were compared with a direct numerical resolution of Eqs. (26) and (28) with $s = j\omega_c(K_c)$, solved with the `fsolve` routine from MATLAB using a homotopy on K_c. Fig. 8 compares the obtained critical delays. For small EEMCFs, the three models agree almost perfectly. Incidentally, this is also the range where the instabilities can be a compelling problem.

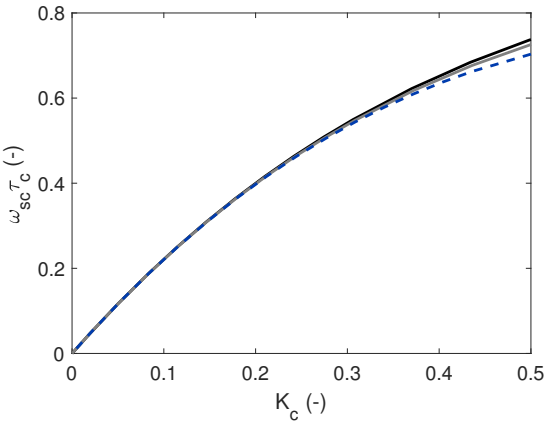

Figure 8. Critical delays τ_c: ZOH model (—), pure delay model (—) and series approximation (- -).

FRF of the controlled system Fig. 9 shows representative FRFs of the controlled system including the ZOH (using Eq. (25)). All the numerical FRFs and frequencies featured in this work are normalized with k_{sc} and ω_{sc}, respectively. Small sampling periods ($\tau \leq 0.1\tau_c$) have an imperceptible effect on the FRF compared to the nominal case. Conversely, a strong effect can be observed for large delays, especially on the rightmost peak whose amplitude grows with the delay. At $\tau = \tau_c$, the poles that lie on the imaginary axis create an undamped resonance in the FRF, signaling the onset of instability. The changes induced by sampling delays on the FRFs are qualitatively similar for both cases, but it should be noted that the critical sampling periods are different, and delay-induced instabilities arise for a sampling period approximately ten times smaller for $K_c = 0.01$ than for $K_c = 0.1$.

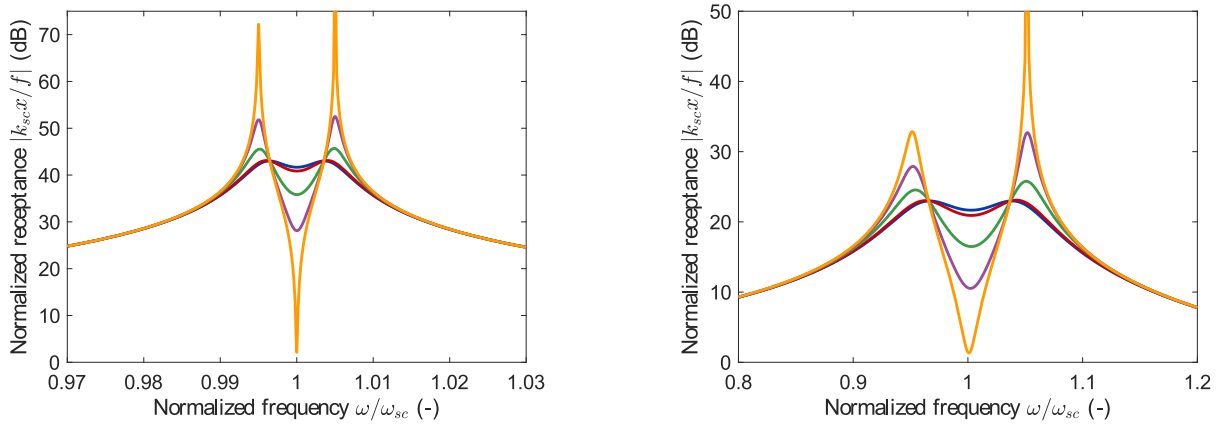

Figure 9. FRF of the controlled system with a delayed admittance, $K_c = 0.01$ (a) and $K_c = 0.1$ (b): $\tau = 0.01\tau_c$ (—), $\tau = 0.1\tau_c$ (—), $\tau = 0.5\tau_c$ (—), $\tau = 0.8\tau_c$ (—) and $\tau = \tau_c$ (—).

The analytical approximations were also verified by time simulations of the systems' responses to a unit-amplitude swept-sine forcing under various sampling frequencies. The simulation of the system represented as a block diagram in Fig. 10 was carried out with Simulink. In addition to the sampling delay, this simulation accounts for the time-varying character of the system caused by sampling, as well as the effect of the discretization of the transfer function with Tustin's method. Fig. 11 shows the envelopes of the systems' responses. The fact that the FRF is nearly not affected for $\tau \leq 0.1\tau_c$ is verified, and so is the progressive degradation, up to the onset of instability for $\tau \approx \tau_c$.

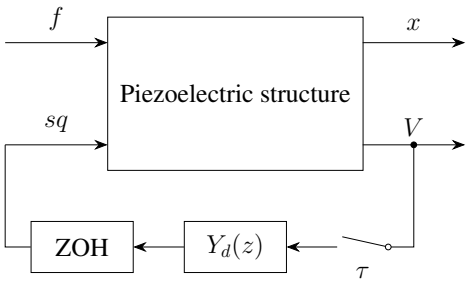

Figure 10. Block diagram representation of the controlled system used for time simulations.

According to the foregoing discussion, a rule of thumb is thus to choose the sampling period lower than or equal to one tenth of the critical delay. Besides, the sampling time must also be small enough so as to respect the Nyquist condition. Typical sampling frequencies of ten to thirty times the highest frequency of interest are often recommended (Franklin et al. 1998). The sampling time should therefore satisfy

$$\tau \leq \frac{1}{\omega_{sc}} \min\left\{\frac{2\pi}{30}, \frac{\sqrt{6}}{10}\left(K_c - K_c^2\right) + \frac{19}{320}\sqrt{\frac{3}{2}}K_c^3\right\}. \tag{34}$$

Stabilization of delay-induced instabilities

Discussion

The delay-induced instabilities are clearly defeating the purpose of the DVA and should therefore be avoided. If the closed-loop system is prone to these instabilities, there are two possible options:

1. Choose a high enough sampling frequency.
2. Modify the implemented admittance in anticipation of the delays.

The first option is the most obvious and straightforward, but not always the most desirable one for two main reasons.

One reason is that a given digital unit's power consumption is a growing function of its clock frequency, which must be high enough to handle data at a given sampling frequency. The power consumption of the MCU can be estimated by (Cardoso et al. 2017)

$$\begin{aligned} P_{\text{MCU}} &= P_{\text{MCU,Static}} + P_{\text{MCU,Dynamic}} \\ &= V_{CC,MCU} I_{CC,MCU} + \beta_{MCU} C_L V_{CC,MCU}^2 f_{CPU} \end{aligned} \tag{35}$$

where $V_{CC,MCU}$ is the supply voltage, $I_{CC,MCU}$ the quiescent current, β_{MCU} is the activity factor, C_L is the load capacitance and f_{CPU} is the clock frequency at which the digital unit is operating. Increasing the sampling frequency will increase β_{MCU} and/or f_{CPU}, leading to a higher power consumption. Moreover, if f_{CPU} is increased, $V_{CC,MCU}$

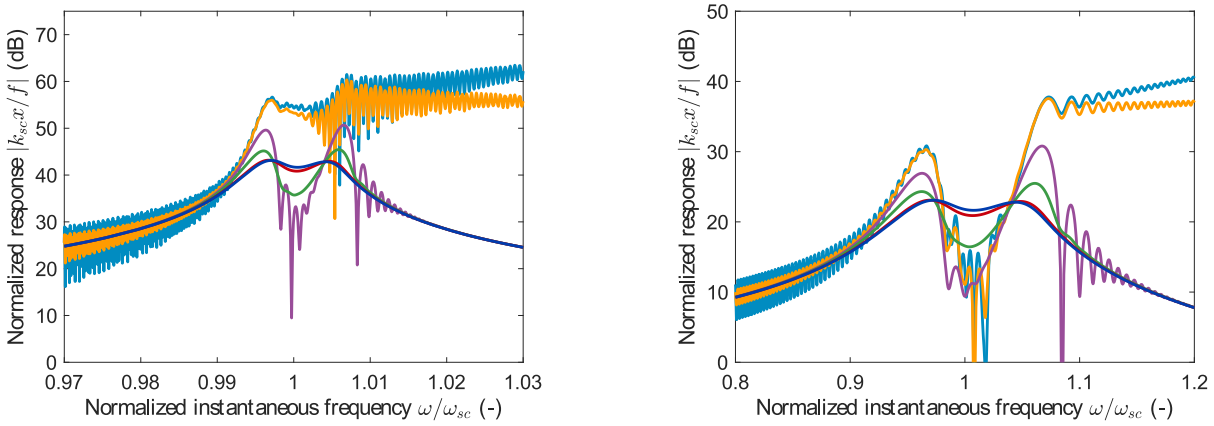

Figure 11. Simulated envelope of the response of the controlled system with a delayed admittance to a unit-amplitude swept sine, $K_c = 0.01$ (a) and $K_c = 0.1$ (b): $\tau = 0.01\tau_c$ (—), $\tau = 0.1\tau_c$ (—), $\tau = 0.5\tau_c$ (—), $\tau = 0.8\tau_c$ (—), $\tau = \tau_c$ (—) and $\tau = 1.01\tau_c$ (—).

will also have to be increased, which leads to an actual power consumption proportional to f_{CPU}^3 (Cardoso et al. 2017).

The second reason is that the required sampling frequency to make the delays effect negligible or let alone to have a stable closed-loop system may be very large. This would require high-frequency specialized equipments, whose cost may become prohibitively large.

Stabilization procedure

The principles of the proposed stabilization procedure are very similar to a pole placement approach: it is sought to place the poles of a modified delayed system as close as possible to those of the nominal system by modifying the parameters of the shunt admittance.

Pole placement via transfer function modification The admittance of a shunt can be expressed as

$$Y_s(s) = \frac{\sum_{m=0}^{M} b_m s^m}{\sum_{n=0}^{N} a_n s^n} \tag{36}$$

According to Eq. (15), the poles of the nominal closed-loop system p_k ($k = 1, \cdots, K$) satisfy

$$1 - \frac{V(p_k)}{p_k q(p_k)} Y_s(p_k) = 0. \tag{37}$$

In order to anticipate the delays, a modified admittance is introduced as

$$\widetilde{Y_s}(s) = \frac{\sum_{m=0}^{M} b_m (1+\delta_{b_m}) s^m}{\sum_{n=0}^{N} a_n (1+\delta_{a_n}) s^n}, \tag{38}$$

where δ_{a_n} and δ_{b_m} are modification factors and are unknown for now. The poles of the modified delayed closed-loop system would be the solutions of Eq. (26):

$$1 - \frac{V(s)}{sq(s)} \frac{1-e^{-\tau s}}{\tau s} \widetilde{Y_s}(s) = 0. \tag{39}$$

By comparing Eqs. (37) and (39), in order for p_k to be a pole of the modified delayed system, the modified delayed admittance must be equal to the nominal one at $s = p_k$:

$$\begin{aligned} \frac{1-e^{-\tau p_k}}{\tau p_k} \widetilde{Y_s}(p_k) &= \frac{1-e^{-\tau p_k}}{\tau p_k} \frac{\sum_{m=0}^{M} b_m (1+\delta_{b_m}) p_k^m}{\sum_{n=0}^{N} a_n (1+\delta_{a_n}) p_k^n} \\ &= \frac{\sum_{m=0}^{M} b_m p_k^m}{\sum_{n=1}^{N} a_n p_k^n} = Y_s(p_k). \end{aligned} \tag{40}$$

Rearranging this equation, the following relation is obtained

$$\begin{aligned} \frac{1-e^{-\tau p_k}}{\tau p_k} \frac{\sum_{m=0}^{M} b_m \delta_{b_m} p_k^m}{\sum_{m=0}^{M} b_m p_k^m} - \frac{\sum_{n=0}^{N} a_n \delta_{a_n} p_k^n}{\sum_{n=0}^{N} a_n p_k^n} \\ = 1 - \frac{1-e^{-\tau p_k}}{\tau p_k}, \end{aligned} \tag{41}$$

which, when imposed for $k = 1, \cdots, K$, defines a linear system that can be put in a matrix form as

$$\begin{bmatrix} \mathbf{B} & \mathbf{A} \end{bmatrix} \begin{bmatrix} \delta_{b_0} \\ \vdots \\ \delta_{b_M} \\ \delta_{a_0} \\ \vdots \\ \delta_{a_N} \end{bmatrix} = \begin{bmatrix} 1 - \dfrac{1-e^{-\tau p_1}}{\tau p_1} \\ \vdots \\ 1 - \dfrac{1-e^{-\tau p_K}}{\tau p_K} \end{bmatrix}, \tag{42}$$

where

$$\mathbf{B} = \begin{bmatrix} \frac{1-e^{-\tau p_1}}{\tau p_1}\frac{b_0}{\sum_{m=0}^{M} b_m p_1^m} & \cdots & \frac{1-e^{-\tau p_1}}{\tau p_1}\frac{b_M p_1^M}{\sum_{m=0}^{M} b_m p_1^m} \\ \vdots & & \vdots \\ \frac{1-e^{-\tau p_K}}{\tau p_K}\frac{b_0}{\sum_{m=0}^{M} b_m p_K^m} & \cdots & \frac{1-e^{-\tau p_K}}{\tau p_K}\frac{b_M p_K^M}{\sum_{m=0}^{M} b_m p_K^m} \end{bmatrix} \tag{43}$$

and

$$\mathbf{A} = \begin{bmatrix} -\frac{a_0}{\sum_{n=0}^{N} a_n p_1^n} & \cdots & -\frac{a_N p_1^N}{\sum_{n=0}^{N} a_n p_1^n} \\ \vdots & & \vdots \\ -\frac{a_0}{\sum_{n=0}^{N} a_n p_K^n} & \cdots & -\frac{a_N p_K^N}{\sum_{n=0}^{N} a_n p_K^n} \end{bmatrix}. \tag{44}$$

In short, Eq. (42) can be rewritten

$$\mathbf{P}\boldsymbol{\delta} = \mathbf{d}. \tag{45}$$

This system has a trivial solution $\boldsymbol{\delta} = [-1, \cdots, -1]^T$. This makes all the coefficients of the modified admittance equal to zero, which clearly is not an acceptable solution. To resolve this, one of the modification factor can be imposed to an arbitrary value, for instance 0. For this particular choice, the column associated with this modification coefficient may simply be removed from $\mathbf{P}$. Thus, the number of unknowns is reduced to $M + N + 1$. Since this number may not be equal to K, the system may not be square. To solve it, the pseudoinverse (denoted by a superscript †) is used.

$$\boldsymbol{\delta} = \mathbf{P}^{\dagger}\mathbf{d}. \tag{46}$$

It should be noted that the procedure only requires the knowledge of the sampling period τ in addition to what is already known for tuning the shunt. This parameter is set by the user and is thus well-known and well-controlled.

Analytical approximations for the series RL shunt

Accurate approximate analytical solutions can be obtained for the case of a delayed series RL shunt. In this case, $b_0 = 1$, $a_0 = R$ and $a_1 = L$. To have a well-posed system, $\delta_{b_0} = 0$ is imposed, while the modifications $\delta_{a_0} = \delta_R$ and $\delta_{a_1} = \delta_L$ on the resistance and inductance, respectively, are sought to stabilize the system. The matrix $\mathbf{A}$ from Eq. (42) reads

$$\mathbf{A} = \begin{bmatrix} -\frac{R}{Lp_1 + R} & -\frac{Lp_1}{Lp_1 + R} \\ \vdots & \vdots \\ -\frac{R}{Lp_4 + R} & -\frac{Lp_4}{Lp_4 + R} \end{bmatrix}, \tag{47}$$

where the poles p_1 to p_4 can in principle be found in closed-form, since the characteristic polynomial is of fourth order. Premultiplication of Eq. (42) by $\mathbf{A}^H$ (where superscript H denotes Hermitian transposition) yields

$$\mathbf{A}^H\mathbf{A}\boldsymbol{\delta} = \mathbf{A}^H\mathbf{d}. \tag{48}$$

This system of two unknowns is solvable in closed-form, but the resulting expressions are impractically long. Alternatively, an approximate solution can be obtained by expanding $\mathbf{A}$ and $\mathbf{d}$ in power series of K_c, and solving Eq. (48) using truncated Laurent series for $\boldsymbol{\delta}$. The software Wolfram Mathematica was once more used to solve Eq. (48) up to $O(K_c^2)$, yielding the series

$$\begin{aligned} \delta_L = {} & \frac{\sin(\tau\omega_{sc})}{\tau\omega_{sc}} - 1 \\ & + \frac{\sqrt{6}}{8}\frac{4\cos(\omega_{sc}\tau) + \tau\omega_{sc}\sin(\omega_{sc}\tau) - 4}{\tau\omega_{sc}}K_c \\ & + \frac{16\tau\omega_{sc}\cos(\tau\omega_{sc}) - 16\sin(\tau\omega_{sc}) - \tau^2\omega_{sc}^2\sin(\tau\omega_{sc})}{32\tau\omega_{sc}}K_c^2 \\ & + O(K_c^3) \end{aligned} \tag{49}$$

and

$$\begin{aligned} \delta_R = {} & \frac{\sqrt{6}}{3}\frac{1-\cos(\tau\omega_{sc})}{\tau\omega_{sc}}\frac{1}{K_c} \\ & + \frac{5\sin(\tau\omega_{sc}) - \tau\omega_{sc}\cos(\tau\omega_{sc}) - 4\tau\omega_{sc}}{4\tau\omega_{sc}} + O(K_c). \end{aligned} \tag{50}$$

Fig. 12 compares the analytical solution given by Eqs. (49) and (50) to the direct numerical solution of the least-squares problem (Eq. (46)). This analytical approximation fits well the numerical solution, even for a fairly large EEMCF. It can also be observed that large increases are necessary for the resistance in case the electromechanical coupling is small, whereas those on the inductance remain moderate for small values of τ. This comes from the term in K_c^{-1} in Eq. (50). Intuitively, this increase in resistance is necessary to compensate for the negative damping effect of the delays highlighted in Figs. 6 and 9. It is also in agreement with what was previously proposed in the literature to stabilize the system (Sugino et al. 2020).

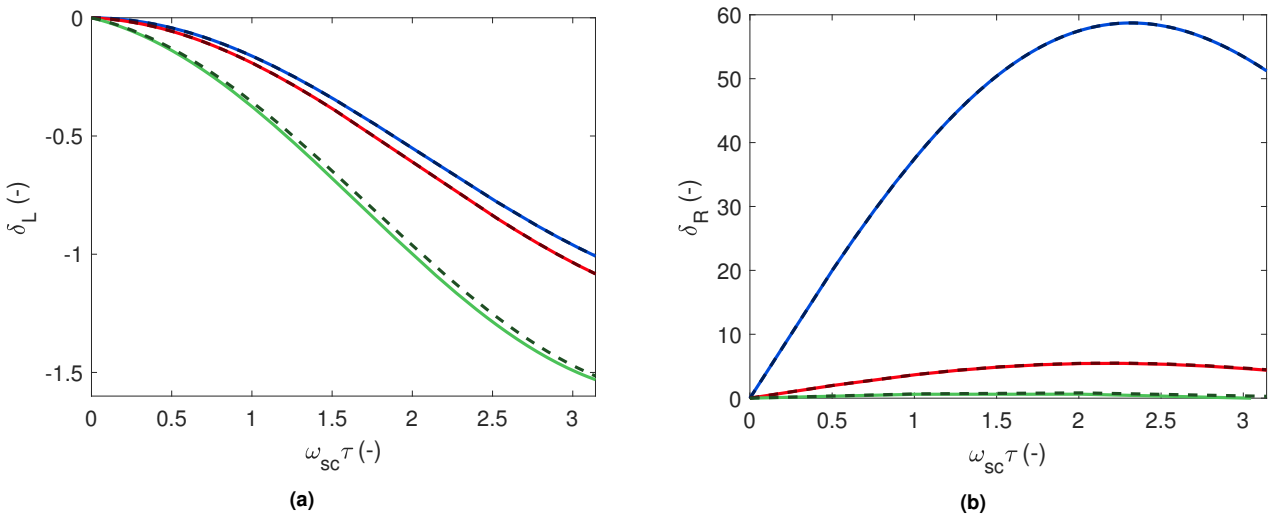

Figure 12. Modification coefficients for the inductance (a) and the resistance (b) (—: numerical solution, - -: series approximation): $K_c = 0.01$ (—), $K_c = 0.1$ (—) and $K_c = 0.5$ (—).

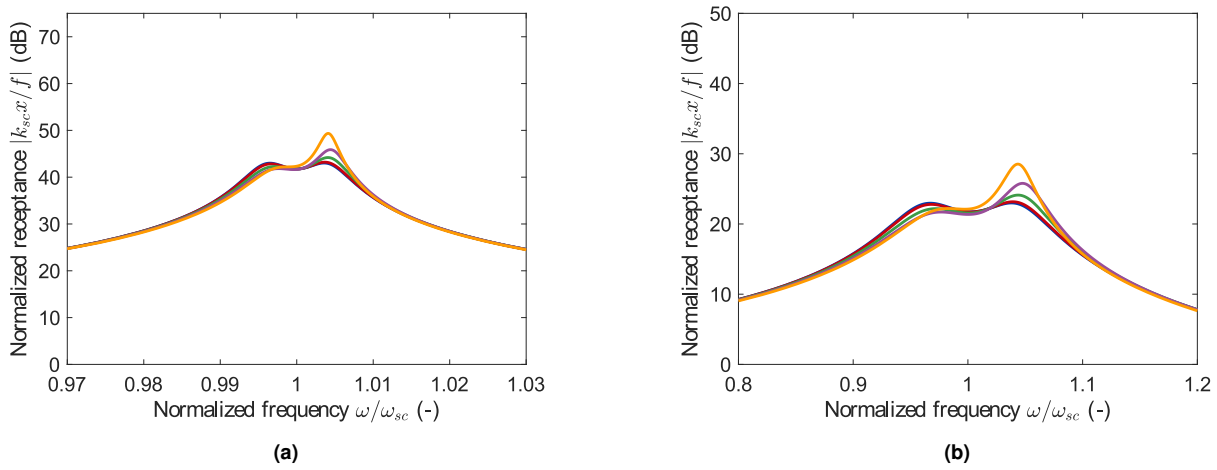

Figure 13. FRF of the controlled system with a modified delayed admittance, $K_c = 0.01$ (a) and $K_c = 0.1$ (b): $\tau = 0.01/\omega_{sc}$ (—), $\tau = 0.1/\omega_{sc}$ (—), $\tau = 0.5/\omega_{sc}$ (—), $\tau = 1/\omega_{sc}$ (—) and $\tau = \pi/\omega_{sc}$ (—).

Numerical verification

$$\tau \leq \frac{2\pi}{30\omega_{sc}} \tag{51}$$

to ensure the stability of the closed-loop system with a modified admittance with some margin.

Experimental validation

Table 1. Parameters of the clamped-free piezoelectric beam with a thin lamina.

l	b	t	l_l	b_l	t_l
700 mm	14 mm	14 mm	40 mm	14 mm	0.5 mm

To identify the system, the FRFs of the beam whith short-circuited and open-circuited patches were measured. Fitting these FRFs gave an estimation of the short- and open-circuit resonance frequencies. The piezoelectric capacitance was then measured with a multimeter (FLUKE 177). From these parameters, the optimal inductance and resistance of a series RL shunt were computed using Eqs. (9) and (10), respectively. All these parameters are reported in Table 3. The DVA shown in Fig. 15(b) was powered with $\pm 25V$, and the MCU was programmed in order to mimic the admittance of the series RL shunt.

Table 2. Parameters of the piezoelectric patches of the clamped-free piezoelectric beam with a thin lamina.

l_p	b_p	t_p	x_0	Δx_p
67 mm	14 mm	2 mm	1 mm	3 mm

To experimentally validate the developments about delay-induced instabilities, FRFs were measured under progressively decreasing sampling frequencies. As testified by Fig. 17(a), the destabilization effect of the sampling frequency is clearly observable. The results featured in this

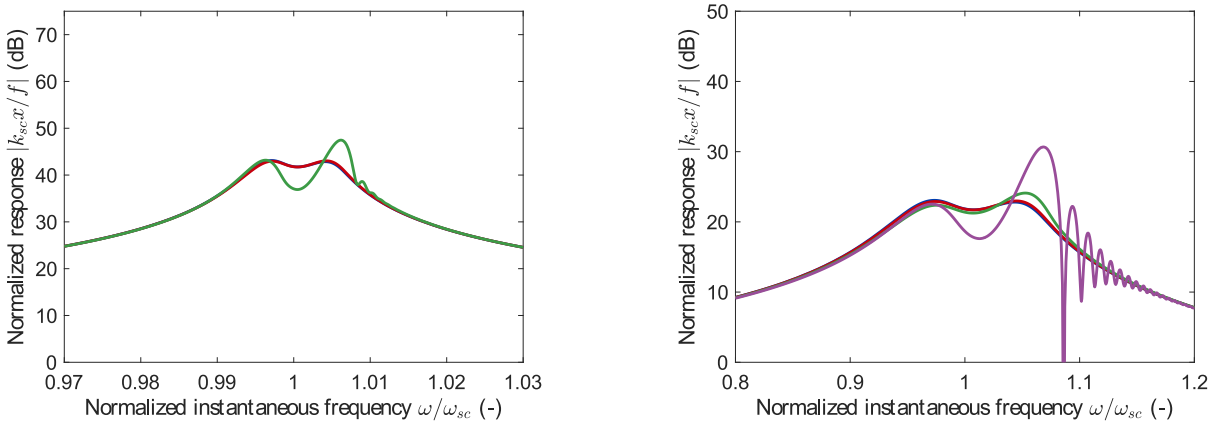

Figure 14. Simulated envelope of the response of the controlled system with a delayed, modified admittance to a unit-amplitude swept sine, $K_c = 0.01$ (a) and $K_c = 0.1$ (b): $\tau = 0.01/\omega_{sc}$ (—), $\tau = 0.1/\omega_{sc}$ (—), $\tau = 0.5/\omega_{sc}$ (—) and $\tau = 1/\omega_{sc}$ (—).

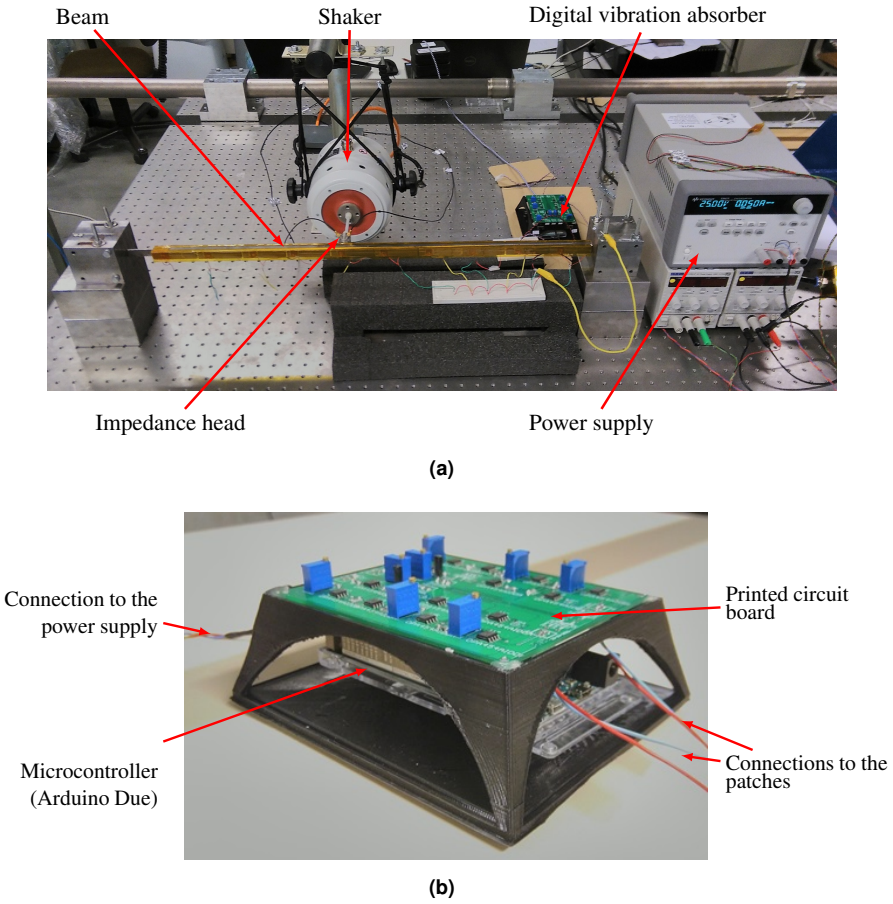

Figure 15. Picture of the experimental setup (a) and close-up on the DVA (b).

Table 3. Parameters of the experimental setup.

Parameter	f_{sc}	f_{oc}	K_c	C_p^ε	R	L
Value	31.08 Hz	31.29 Hz	0.116	245 nF	2,961 Ω	105.7 H

figure are close to those of Fig. 9(b) (the coupling factor of the experimental setup is 0.116, which is close to the EEMCF of 0.1 used therein), which validates the model used to describe sampling delays. From Eq. (33), the stability limit of the unmodified system should theoretically be reached at $\tau = 1.3 \times 10^{-3}$s. The experimental system is still stable but very lightly damped. This small discrepancy can be explained by the presence of structural damping in the host, as well as by experimental uncertainties.

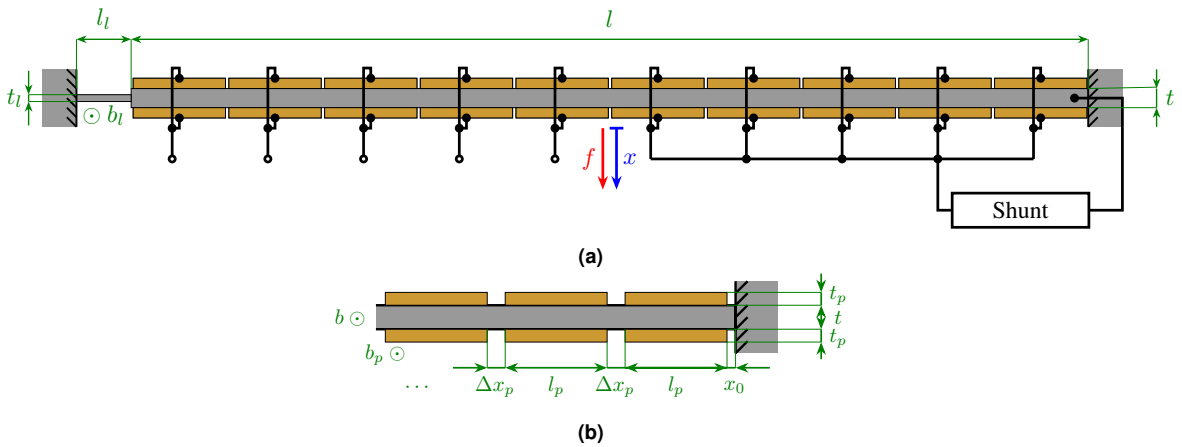

Figure 16. Schematic representation of the clamped-free piezoelectric beam with a thin lamina: overall view (a) and close-up on the patches close to the clamped end (b).

The stabilization procedure recovers the performance of a case without delays, as shown in Fig. 17(b). Namely, all the curves are virtually superimposed up to $\tau = \tau_c$, which validates the proposed stabilization method. Fourfold a sampling period leads to a system with modified admittance where the effects of sampling are observable, more than in the numerical model featured in Fig. 13(b), but similarly to the time simulation in Fig. 14(b). Nevertheless, a case with such a high sampling period when the admittance is unmodified is not disclosed here, as it leads to an unstable closed-loop system.

Conclusion

A DVA used for piezoelectric shunt damping is an attractive solution but it may be hindered by delay-induced instabilities incurred by the sampling procedure in the digital unit. After reviewing the basics of piezoelectric shunt damping with a DVA, this work used concepts from feedback control theory to highlight the small phase margin exhibited by piezoelectric systems with small EEMCFs. This makes them susceptible to delay-induced instabilities when a DVA is used, despite the passive character of the control law. An approximate explicit relation was derived between the maximum sampling period guaranteeing stability and the EEMCF, and it was shown that this period tends to zero concurrently with the EEMCF.

The developments were experimentally validated on a piezoelectric beam controlled by a DVA. Namely, it was shown that the expression for the maximum sampling period for stability is accurate, and that the stabilization procedure leads to a controlled system which behaves similarly to a piezoelectric structure with a shunt.

Funding

This work was supported by the SPW [WALInnov grant 1610122].

References

Berardengo M, Manzoni S, Thomas O and Vanali M (2018) Piezoelectric resonant shunt enhancement by negative capacitances: Optimisation, performance and resonance cancellation. *Journal of Intelligent Material Systems and Structures* 29(12): 2581–2606. DOI:10.1177/1045389X18770874. URL https://doi.org/10.1177/1045389X18770874.

Cardoso JM, Coutinho JGF and Diniz PC (2017) *Embedded Computing for High Performance*. Elsevier. ISBN 9780128041895. DOI:10.1016/C2015-0-00283-0. URL https://linkinghub.elsevier.com/retrieve/pii/C20150002830.

Dal Bo L, Gardonio P, Casagrande D and Saggini S (2019) Smart panel with sweeping and switching piezoelectric patch vibration absorbers: Experimental results. *Mechanical Systems and Signal Processing* 120: 308–325. DOI:10.1016/j.ymssp.2018.10.024. URL https://doi.org/10.1016/j.ymssp.2018.10.024https://linkinghub.elsevier.com/retrieve/pii/S0888327018306927.

Fleming A, Behrens S and Moheimani S (2000) Synthetic impedance for implementation of piezoelectric shunt-damping circuits. *Electronics Letters* 36(18): 1525. DOI:10.1049/el:20001083. URL https://digital-library.theiet.org/content/journals/10.1049/el{_}20001083.

Fleming A and Moheimani S (2002) Power Harvesting Piezoelectric Shunt Damping 1. *IFAC Proceedings Volumes* 35(2): 173–178. DOI:10.1016/S1474-6670(17)33937-X. URL

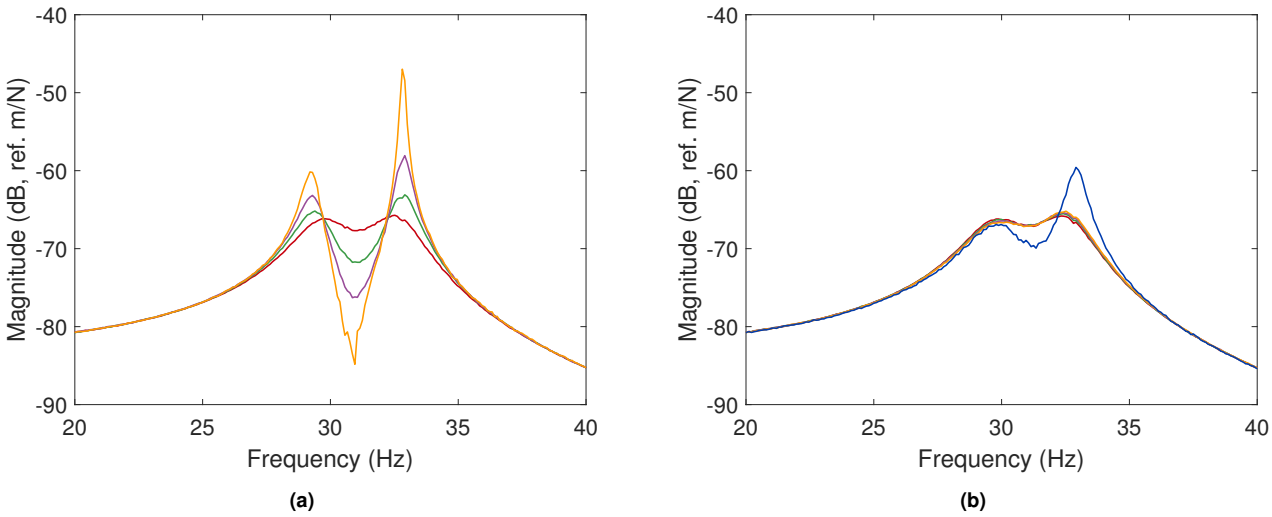

Figure 17. Experimental FRF of the beam ($K_c = 0.116$) with an unmodified (a) and a modified (b) admittance: $\tau = 10^{-4}$s$\approx 0.1\tau_c$ (—), $\tau = 6.5 \times 10^{-4}s= 0.5\tau_c$ (—), $\tau = 10^{-3}$s$\approx 0.8\tau_c$ (—), $\tau = 1.3 \times 10^{-3}s= \tau_c$ (—) and $\tau = 5 \times 10^{-3}$s$\approx 1/\omega_{sc}$ (—) .

https://linkinghub.elsevier.com/retrieve/pii/S147466701733937X.

Fleming AJ (2004) *Synthesis and Implementation of Sensor-less Shunt Controllers for Piezoelectric and Electromagnetic Vibration Control*. PhD Thesis, University of Newcastle. URL http://www.precisionmechatronicslab.com/wp-content/uploads/2017/11/10.1.1.386.3374.pdf.

Forward RL (1979) Electronic damping of vibrations in optical structures. *Applied Optics* 18(5): 690. DOI:10.1364/AO.18.000690. URL https://www.osapublishing.org/abstract.cfm?URI=ao-18-5-690.

Franklin GF, Powell JD and Emami-Naeini A (2015) *Feedback Control of Dynamic Systems*. Pearson London. ISBN 978-0-13-468571-7.

Franklin GF, Powell JD and Workman ML (1998) *Digital Control of Dynamic Systems*. 3 edition. Addison-wesley Reading, MA. ISBN 978-0201820546.

Giorgio I, Culla A and Del Vescovo D (2009) Multi-mode vibration control using several piezoelectric transducers shunted with a multiterminal network. *Archive of Applied Mechanics* 79(9): 859–879. DOI:10.1007/s00419-008-0258-x. URL http://link.springer.com/10.1007/s00419-008-0258-x.

Hagood N and von Flotow A (1991) Damping of structural vibrations with piezoelectric materials and passive electrical networks. *Journal of Sound and Vibration* 146(2): 243–268. DOI:10.1016/0022-460X(91)90762-9. URL https://linkinghub.elsevier.com/retrieve/pii/0022460X91907629.

Høgsberg J and Krenk S (2017) Calibration of piezoelectric RL shunts with explicit residual mode correction. *Journal of Sound and Vibration* 386: 65–81. DOI:10.1016/j.jsv.2016.08.028. URL http://dx.doi.org/10.1016/j.jsv.2016.08.028.

Ikegame T, Takagi K and Inoue T (2019) Exact Solutions to H∞ and H2 Optimizations of Passive Resonant Shunt Circuit for Electromagnetic or Piezoelectric Shunt Damper. *Journal of Vibration and Acoustics* 141(3): 031015. DOI:10.1115/1.4042819. URL https://asmedigitalcollection.asme.org/vibrationacoustics/article/doi/10.1115/1.4042819/727600/Exact-Solutions-to-H-and-H2-Optimizations-of.

Matten G, Collet M, Cogan S and Sadoulet-Reboul E (2014) Synthetic Impedance for Adaptive Piezoelectric Metacomposite. *Procedia Technology* 15: 84–89. DOI:10.1016/j.protcy.2014.09.037. URL https://linkinghub.elsevier.com/retrieve/pii/S2212017314001522.

Moheimani SOR, Fleming AJ and Behrens S (2003) On the feedback structure of wideband piezoelectric shunt damping systems. *Smart Materials and Structures* 12(1): 49–56. DOI:10.1088/0964-1726/12/1/306. URL https://iopscience.iop.org/article/10.1088/0964-1726/12/1/306.

Nečásek J, Václavík J, and Marton P (2017) Comparison of analog front-ends for digital synthetic impedance device. In: *2017 IEEE International Workshop of Electronics, Control, Measurement, Signals and their Application to Mechatronics (ECMSM)*. IEEE. ISBN 978-1-5090-5582-1, pp. 1–4. DOI:10.1109/ECMSM.2017.7945916. URL http://ieeexplore.ieee.org/document/7945916/.

Nečásek J, Václavík J and Marton P (2016) Digital synthetic impedance for application in vibration damping. *Review of Scientific Instruments* 87(2): 024704. DOI:10.1063/1.

4942085. URL http://aip.scitation.org/doi/10.1063/1.4942085.

Niederberger D, Fleming A, Moheimani SOR and Morari M (2004) Adaptive multi-mode resonant piezoelectric shunt damping. *Smart Materials and Structures* 13(5): 1025–1035. DOI:10.1088/0964-1726/13/5/007. URL https://iopscience.iop.org/article/10.1088/0964-1726/13/5/007.

Olgac N and Elmali H (2000) Analysis and Design of Delayed Resonator in Discrete Domain. *Journal of Vibration and Control* 6(2): 273–289. DOI:10.1177/107754630000600207. URL http://journals.sagepub.com/doi/10.1177/107754630000600207.

Plíva Z, Kolář M, Došek P and Sluka T (2007) A Piezoelectric Elements and Their Electronics Driving with Help of FPGA Circuits. *Ferroelectrics* 351(1): 187–195. DOI:10.1080/00150190701354273. URL http://www.tandfonline.com/doi/abs/10.1080/00150190701354273.

Preumont A (2011) *Vibration Control of Active Structures*, *Solid Mechanics and Its Applications*, volume 179. 3 edition. Dordrecht: Springer Netherlands. ISBN 978-94-007-2032-9. DOI:10.1007/978-94-007-2033-6. URL http://link.springer.com/10.1007/978-94-007-2033-6.

Raze G, Jadoul A, Guichaux S, Broun V and Kerschen G (2020) A digital nonlinear piezoelectric tuned vibration absorber. *Smart Materials and Structures* 29(1): 015007. DOI:10.1088/1361-665X/ab5176. URL https://iopscience.iop.org/article/10.1088/1361-665X/ab5176.

Raze G, Paknejad A, Zhao G, Broun V, Collette C and Kerschen G (2019) Suppression of delay-induced instabilities of digital piezoelectric vibration absorbers. In: Benjeddou A, Mechbal N and Deü JF (eds.) *Proceedings of the 9th ECCOMAS Thematic Conference on Smart Structures and Materials - SMART 2019*. International Centre for Numerical Methods in Engineering (CIMNE), pp. 991–1001. URL http://hdl.handle.net/2268/240342.

Rosi G (2010) *Control of sound radiation and transmission by means of passive piezoelectric networks : modelling , optimization and experimental implementation*. PhD Thesis, Université Pierre et Marie Curie - Paris VI. URL https://tel.archives-ouvertes.fr/tel-00815038.

Silva TMP (2018) *Vibration attenuation in linear and nonlinear flexible structures via nonlinear piezoelectric shunt circuits*. PhD Thesis, University of São Paulo.

Soltani P, Kerschen G, Tondreau G and Deraemaeker A (2014) Piezoelectric vibration damping using resonant shunt circuits: an exact solution. *Smart Materials and Structures* 23(12): 125014. DOI:10.1088/0964-1726/23/12/125014. URL http://stacks.iop.org/0964-1726/23/i=12/a=125014?key=crossref.798743ce34b627bed945b046d8a6b51a.

Sugino C, Ruzzene M and Erturk A (2018) Design and Analysis of Piezoelectric Metamaterial Beams with Synthetic Impedance Shunt Circuits. *IEEE/ASME Transactions on Mechatronics* 23(5): 2144–2155. DOI:10.1109/TMECH.2018.2863257.

Sugino C, Ruzzene M and Erturk A (2020) Digitally Programmable Resonant Elastic Metamaterials. *Physical Review Applied* 13(6): 1. DOI:10.1103/physrevapplied.13.061001. URL https://doi.org/10.1103/PhysRevApplied.13.061001.

Thomas O, Ducarne J and Deü JF (2012) Performance of piezoelectric shunts for vibration reduction. *Smart Materials and Structures* 21(1): 015008. DOI:10.1088/0964-1726/21/1/015008. URL http://stacks.iop.org/0964-1726/21/i=1/a=015008?key=crossref.6d8696aab65a8889d18c15289623f766.

Tustin A (1947) A method of analysing the behaviour of linear systems in terms of time series. *Journal of the Institution of Electrical Engineers - Part IIA: Automatic Regulators and Servo Mechanisms* 94(1): 130–142. DOI:10.1049/ji-2a.1947.0020. URL https://digital-library.theiet.org/content/journals/10.1049/ji-2a.1947.0020.

Walton K and Marshall J (1987) Direct method for TDS stability analysis. *IEE Proceedings D Control Theory and Applications* 134(2): 101. DOI:10.1049/ip-d.1987.0018. URL https://digital-library.theiet.org/content/journals/10.1049/ip-d.1987.0018.

Yi K, Matten G, Ouisse M, Sadoulet-Reboul E, Collet M and Chevallier G (2020) Programmable metamaterials with digital synthetic impedance circuits for vibration control. *Smart Materials and Structures* 29(3): 035005. DOI:10.1088/1361-665X/ab6693. URL https://iopscience.iop.org/article/10.1088/1361-665X/ab6693.